ELSEVIER

Chemical Engineering Journal 134 (2007) 131–137

Chemical Engineering Journal

www.elsevier.com/locate/cej

Modeling of a heat-coupled catalytic reactor with co-current oxidation and conversion flows

V.A. Kirillov [a], S.I. Fadeev [b], N.A. Kuzin [a], A.B. Shigarov [a,*]

[a] *Boreskov Institute of Catalysis, Prosp. Akad. Lavrentieva 5, Novosibirsk 630090, Russia*
[b] *Sobolev Institute of Mathematics, Prosp. Akad. Koptyuga 4, Novosibirsk 630090, Russia*

Abstract

Mathematical model and numerical method are developed to analyze the operation of a coupled methane steam reformer. The reformer operates in co-current mode of endothermic (steam reforming) and exothermic (fuel oxidation) departments. The exhaust anode gas of a fuel-cell battery containing hydrogen is used as fuel. Two-dimensional, two-temperature mathematical model of monolith is used to describe processes in exothermic and endothermic departments of the reformer. Calculation results were compared with experiments. The agreement between the modeling and the experimental results is rather good. The model analysis points out that the considered reactor design has high parametric sensitivity, there is a probability of arisen of a hysteresis with points of ignition and extinction.

Keywords: Methane steam reforming; Hydrogen combustion; Heat coupling of exothermic and endothermic reactions; Structured catalyst; Reactor modeling

1. Introduction

Development of a compact catalytic reactor for conversion of hydrocarbons into synthesis gas (for on-board hydrogen production for fuel cells on transport vehicles) has become a highly topical problem in recent years. Steam reforming provides the maximal hydrogen content in synthesis gas (in comparison with partial oxidation or autothermal reforming), but it is highly endothermic reaction and requires effective heat supply to the reaction zone. One of the possible solutions of this problem is heat coupling (integration in one reactor) of the hydrocarbon steam reforming and catalytic combustion of the same hydrocarbon or, more advantageous, of exhaust/anode gas (mainly hydrogen) from the fuel-cell battery. Various types of such reactors have been developed. Here we restrict our consideration only by an item of the mathematical simulation of a coupled-by-heat reactor. A limited number of such studies are known (see, for example [1–6]). One-dimensional two-phase model of autothermal monolith reactor with counter-current operation for methane steam reforming and combustion is suggested [1]. The results of CFD-simulation of catalytic plate reactors for the same reaction system but with co-current operation are reported in [2,3]. Coupled steam reforming of octane and catalytic combustion of hydrogen with co-current operation in microchannel reactor is investigated in [4]. Among these papers, the only [4–6] presented some comparison between modeling and experimental data. The main difference between the considered in this paper type of reactor and the ones that are mentioned above, is an originally designed structured metal porous catalyst block for endothermic reaction (so called "endoblock"). A distinguishing feature of this design is compactness at high specific surface of the catalyst block. The catalyst block is formed by sintering of a stack of alternating corrugated and flat thin catalyst sheets on base of a mixture of metal Ni powder and industrial reforming catalyst. Despite of high heat conductivity of the catalyst material, the lateral catalyst bed conductivity is restricted due to high porosity and as consequence high concentrations and temperature gradients across of the block are possible. This last one strongly complicates the mathematical model calculations.

In this work we developed a significantly more sophisticated mathematical model of the coupled by heat reactor as compared to our previous studies [5,6]. The following new features were taken into account:

- temperature difference between the gas flow and the structured catalyst;
- axial heat conductivity along the metallic baffle which separates the endoblock and exothermic block (exochannel);
- kinetics of H_2 oxidation reaction on the walls of exochannel.

* Corresponding author. Tel.: +7 3833306187; fax: +7 3833306187.
E-mail address: shigarov@catalysis.ru (A.B. Shigarov).

1385-8947/$ – see front matter © 2007 Elsevier B.V. All rights reserved.
doi:10.1016/j.cej.2007.03.050

Nomenclature

$b_2^0 = 8.12 \times 10^3$, $b_3^0 = 1.82 \times 10^7$ adsorption equilibrium constants for hydrogen [6], bar^{-1}, bar^{-2}
c_p^{ex}, c_p^{en}, c_p^j, c_p^i heat capacity of gas mixture and its components, J/(kg K)
$C_{cat} = 200$ industrial catalyst content per unit of volume of the endoblock, kg/m^3
$d_{en} = 0.002$ hydraulic diameter of channels in the endoblock, m
$d_{ex} = 0.002$ hydraulic diameter of the exochannel, m
$D_{H_2}^{ex}$ hydrogen–nitrogen diffusion coefficient (temperature dependent), m^2/s
$E_{con} = 1.41 \times 10^5$ activation energy of CH_4 steam reforming [6], J/mol
$E_{H_2} = 2.6 \times 10^4$ activation energy of H_2 oxidation reaction in the exochannel, J/mol
g half mass velocity of gas in the exochannel (per unit width), kg/(m s)
G_{en} superficial mass velocity of gas in the endoblock, $kg/(m^2\ s)$
$H = 0.005$ half thickness of endoblock, m
$\Delta H_{con} = -2.06 \times 10^5$ heat effect of methane steam reforming reaction, J/mol
$\Delta H_{H_2} = 2.42 \times 10^5$ heat effect of hydrogen oxidation reaction, J/mol
$\Delta H_{sh} = 4.1 \times 10^4$ heat effect of shift-reaction, J/mol
k_{con}, k_{sh} reaction rate constants for CH_4 steam reforming and shift-reaction, $mol/(m^3\ s\ bar)$
$k_{con}^0 = 2 \times 10^{12}$ preexponential factor for CH_4 steam reforming rate [6], $mol/(m^2\ s\ bar)$
k_{ox} reaction rate constant for hydrogen oxidation, m/s
k_{ox}^0 preexponential factor for hydrogen oxidation rate, m/s
$k_{sh}^0 = 10^4$ preexponential factor for shift-reaction rate [6], $mol/(m^2\ s\ bar)$
K_e^{con}, K_e^{sh} thermodynamic equilibrium constants (temperature dependent) for CH_4 steam conversion and shift-reaction, bar^2
ℓ coordinate along the reactor length, m
$L = 0.2$ reactor length, m
m_i mole mass of gas components, kg/mol
$Nu^{en} = 2.7$ Nusselt number for stabilized laminar flow in the triangular channels of the endoblock
$Nu^{ex} = Sh^{ex} = 8$ Nusselt and Sherwood numbers for stabilized laminar flow in the flat exochannel
P, P_i total and partial pressure, bar
$Q_2 = 8.18 \times 10^4$, $Q_3 = 1.96 \times 10^5$ heats of hydrogen adsorption [6], J/mol
$R_g = 8.31$ ideal gas constant, J/(mol K)
$S = 1200$ specific external surface of the structured catalyst in the endoblock, m^{-1}
$S_{Ni} = 2500$ specific Ni surface for industrial catalyst, m^2/kg
$T_c(\ell, z)$ catalyst temperature, K or °C
$T_g^{en}(\ell, z)$ gas temperature at the endoblock, K or °C
$T_g^{ex}(\ell)$ gas temperature at the exochannel, K or °C
$T_W(\ell) = T_c(\ell, H)$ temperature of the wall between the endoblock and exochannel, K or °C
$w_{H_2}^{ex}$ specific rate of H_2 oxidation (per unit surface of the exochannel wall), $mol/(m^2\ s)$
W_{con} specific rate of CH_4 steam reforming (per unit of volume of the endoblock), $mol/(m^3\ s)$
W_{sh} specific rate of shift-reaction (per unit of volume of the endoblock), $mol/(m^3\ s)$
$x_j(\ell)$ mass fractions of gas components in the exochannel
$x_j^m(\ell)$ mole fractions of gas components in the exochannel
$y_i(\ell, z)$ mass fractions of gas components in the endoblock
$y_i^m(\ell, z)$ mole fractions of gas components in the endoblock
z transverse coordinate (for endoblock), m

Greek symbols

α_{en}, α_{ex} gas–solid heat transfer coefficients for endoblock and exochannel, $W/(m^2\ K)$
$\beta_{H_2}^{ex}$ coefficient of gas-wall mass transfer for hydrogen in the exochannel, m/s
$\delta_{ex} = 0.001$ height of the plane exochannel (distance between the plates), m
$\delta_W = 0.001$ thickness of the wall between the endoblock and exochannel, m
$\lambda_z = 2$ coefficient of transverse thermal conductivity of the endoblock, W/(m K)
λ_g^{ex}, λ_i^{ex}, λ_g^{en}, λ_j^{en} coefficients (temperature dependent) of gas mixture and components thermal conductivity in the exochannel and endoblock, W/(m K)
$\lambda_W = 40$ coefficient of thermal conductivity of the steel wall between the endoblock and the exochannel, W/(m K)
ν stoichiometric reaction coefficients

The novel mathematical formulation required the development of comprehensive numerical method. Besides of comparison of modeling results with experimental data there were analyzed possible critical phenomena and hysteresis during operation of the considered reactor. Finally, some practical conclusions were drawn from the results of modeling.

2. Experimental

2.1. Reactions

We consider the coupling of the combustion of hydrogen on Pt catalyst:

$$H_2 + \tfrac{1}{2}O_2 = H_2O, \quad \Delta H_{298} = -242\ kJ/mol$$

with the steam reforming of methane on Ni catalyst, accompanied by shift-reaction:

$$CH_4 + H_2O = CO + 3H_2, \quad \Delta H_{298} = 206\,\text{kJ/mol}$$

$$CO + H_2O = CO_2 + H_2, \quad \Delta H_{298} = -41\,\text{kJ/mol}$$

As it is seen from the comparison of the heats of reactions, combusting 1 mol of H_2 generates enough heat to produce (by CH_4 steam reforming) approximately 3.5 mol of H_2 (neglected shift-reaction) or 5.9 mol of H_2 (completed shift-reaction). Nevertheless, the demands for heating both exothermic and endothermic gas flows (from its inlet temperatures up to the reaction temperature ~800 °C) and also heat losses may significantly decrease this number. So, heat recuperation may be the solution to make the considered process of hydrogen production more effective, but this question will not be discussed here.

2.2. Reactor structure

Fig. 1 schematically shows the reactor. The size of the experimental reactor: the thickness of metal plate walls—1 mm; the thickness of the hydrogen oxidation catalyst layer adhered to the plate inner surface—1 mm; the thickness of the Ni catalyst layer with regular structure applied to the plate outer side—10 mm; the length of the reactor—200 mm; the number of conjugated units (endoblock + exochannel) in transverse direction—5; the volume—500 cm^3. The experimental conditions used for modeling were: natural gas flow rate 60 cm^3/s, steam—370 cm^3/s, hydrogen—310 cm^3/s and air—2250 cm^3/s. The experiment was described in more details elsewhere [5,6].

2.3. Catalyst

Structured catalysts based on the reinforced porous metal supports were used. Such supports provide enhanced heat transfer between the exothermic and endothermic zones. Catalyst for CH_4 steam reforming was prepared by means of sintering a mixture of 84% powdered Ni and industrial Ni/Al_2O_3 catalyst in reducing atmosphere. The alternating flat and corrugated sheets of the catalyst were stacked up to form a monolith blocks

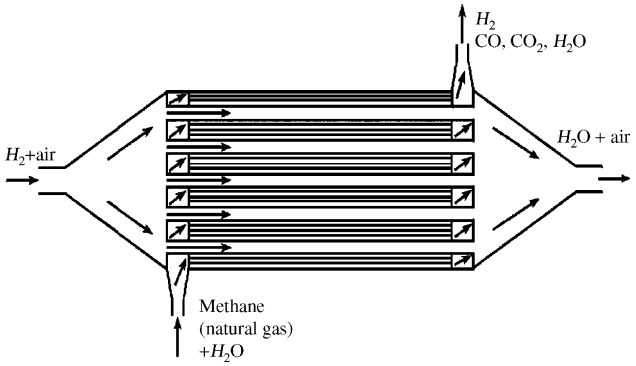

Fig. 1. The scheme of a heat-coupled reactor.

desired dimensions. Catalyst for H_2 oxidation (79.4% Ni^+ 20% Al^+ industrial 0.6% Pt/Al_2O_3 catalyst) was supported on channel walls of the exothermic block. The detailed technique of catalysts preparation is given elsewhere [6].

3. Mathematical model

For the endoblock we consider two-dimensional model in order to be able to calculate accurately the transversal temperature and concentration profile across the endoblock. This model takes into account axial convective mass and heat transfer by gas flow and transversal heat conductivity through the catalyst structure. For the exochannel we take one-dimensional two-temperature model with axial convective mass and heat transfer by gas flow and axial heat conductivity along the wall, which divides endoblock and exochannel. Both sub-models are linked together by equality of temperatures and heat fluxes at the boundary (wall).

Equations of heat and material balance for endoblock:

$$0 \le z \le H, \quad 0 \le \ell \le L,$$

$$c_p^{\text{en}} G_{\text{en}} \frac{\partial T_{\text{g}}^{\text{en}}}{\partial \ell} = \alpha_{\text{en}} S (T_{\text{c}} - T_{\text{g}}^{\text{en}}),$$

$$\lambda_z \frac{\partial^2 T_{\text{c}}}{\partial z^2} + \Delta H_{\text{con}} W_{\text{con}} + \Delta H_{\text{sh}} W_{\text{sh}} = \alpha_{\text{en}} S (T_{\text{c}} - T_{\text{g}}^{\text{en}}),$$

$$G_{\text{en}} \frac{\partial y_i}{\partial \ell} = (\nu_i^{\text{con}} W_{\text{con}} + \nu_i^{\text{sh}} W_{\text{sh}}) m_i,$$

$$i = \{CH_4, H_2O, CO, H_2, CO_2\}, \tag{1}$$

Equations of heat and material balance for exochannel:

$$z = H, \quad 0 \le \ell \le L,$$

$$c_p^{\text{ex}} g \frac{\mathrm{d}T_{\text{g}}^{\text{ex}}}{\mathrm{d}\ell} = \alpha_{\text{ex}} (T_W - T_{\text{g}}^{\text{ex}}),$$

$$g \frac{\mathrm{d}x_j}{\mathrm{d}\ell} = \nu_j^{\text{hyd}} w_{H_2}^{\text{ex}} m_j, \quad j = \{O_2, N_2, H_2, H_2O\}, \tag{2}$$

Equation of heat balance for the wall between endoblock and exochannel:

$$z = H, \quad 0 \le \ell \le L,$$

$$\lambda_z \frac{\partial T_{\text{c}}}{\partial z} + \alpha_{\text{ex}} (T_{\text{W}} - T_{\text{g}}^{\text{ex}}) = w_{H_2}^{\text{ex}} \Delta H_{H_2} + \lambda_{\text{W}} \delta_{\text{W}} \frac{\mathrm{d}^2 T_{\text{W}}}{\mathrm{d}\ell^2}. \tag{3}$$

Boundary conditions:

$$\text{at } \ell = 0: \quad \frac{\mathrm{d}T_{\text{W}}}{\mathrm{d}\ell} = 0, \; T_{\text{g}}^{\text{en}} = T_{\text{g0}}^{\text{en}},$$

$$T_{\text{g}}^{\text{ex}} = T_{\text{g0}}^{\text{ex}}, \; y_i = y_{i0}, \; x_j = x_{j0}; \qquad \text{at } z = 0: \quad \frac{\partial T_{\text{c}}}{\partial z} = 0;$$

$$\text{at } z = H: \quad T_{\text{c}} = T_{\text{W}}; \qquad \text{at } \ell = L: \quad \frac{\mathrm{d}T_{\text{W}}}{\mathrm{d}\ell} = 0. \tag{4}$$

Gas-surface mass and heat transfer:

$$\beta_{H_2}^{ex} = \frac{Sh^{ex} D_{H_2}^{ex}}{d_{ex}}, \qquad \alpha_{ex} = \frac{Nu^{ex}\lambda_g^{ex}}{d_{ex}},$$

$$d_{ex} = 2\delta_{ex},\ \lambda_g^{ex} = \sum_j x_j^m \lambda_j^{ex},\ j = \{O_2, N_2, H_2, H_2O\}.$$

$$\alpha_{en} = \frac{Nu^{en}\lambda_g^{en}}{d_{en}},$$

$$\lambda_g^{en} = \sum_i y_i^m \lambda_i^{en},\ i = \{H_2O, CH_4, H_2, CO, CO_2\}.$$

Kinetic expression for steam reforming of methane on Ni catalyst [7]:

$$W_{con} = \frac{k_{con} P_{CH_4} P_{H_2O}[1 - (P_{CO}(P_{H_2})^3/K_e^{con} P_{CH_4} P_{H_2O})]}{P_{H_2O} + b_2(P_{H_2})^2 + b_3(P_{H_2})^3},$$

$$k_{con} = k_{con}^0 \frac{\exp(-E_{con}/R_g T_c)}{T_c^3} C_{cat} S_{Ni},\ b_2 = b_2^0 \frac{\exp(Q_2/R_g T_c)}{T_c^3},$$

$$b_3 = b_3^0 \frac{\exp(Q_3/R_g T_c)}{T_c^{6.5}},$$

Shift-reaction under considered conditions is reported [7] to be fast enough, thus the equilibrium assumption is valid. So, the formal kinetic expression may be used with arbitrary (but sufficiently high) value of reaction constant k_{sh}:

$$W_{sh} = k_{sh} P_{CO}\left(1 - \frac{P_{CO_2} P_{H_2}}{K_e^{sh} P_{CO} P_{H_2O}}\right), \quad k_{sh} = k_{sh}^0 C_{cat} S_{Ni}$$

Hydrogen combustion on Pt-catalysts is known to be extremely fast. That is why kinetic studies of this system are rare. The study [8] employed the multi-step kinetic approach to show that catalytic washcoat thicker than approximately 100 μm operates in the intracatalyst diffusion region. Therefore, in this paper the simplified first order intra-diffusion kinetics was adopted. This kinetics was derived from the original experimental data [9] that was obtained for 0.5–1 mm fraction of 0.5% Pt/Al_2O_3 catalyst in the circulation-loop reactor. When the interphase (gas–solid) transfer resistance is additionally taken into account, then the resulting expression for the apparent rate of hydrogen oxidation takes the form:

$$\omega_{H_2}^{ex} = \left(\frac{P \times 10^5}{R_g T_g^{ex}}\right) x_{H_2}^m \left(\frac{k_{ox}\beta_{H_2}^{ex}}{\beta_{H_2}^{ex} + k_{ox}}\right),$$

$$k_{ox} = k_{ox}^0 \exp\left(\frac{-E_{H_2}}{R_g T_W}\right).$$

4. Numerical method

The boundary-value problem (1)–(4) does not belong to a standard type. Therefore, the problem solution called for the development of an original numerical method. Below the essential points of this method are briefly discussed.

(1) Finite-difference approximation of the boundary-value problem (1)–(4) is based on the method of lines under uniform discretization of the interval [0, H] and substitution of finite-difference analog of the second derivative of T_c into Eq. (1):

$$\frac{\partial^2 T_c}{\partial z^2}(z_i) \approx \frac{T_c(z_{i-1}) - 2T_c(z_i) + T(z_{i+1})}{\Delta^2},$$

$$\Delta = \frac{H}{M},\ z_j = \Delta(j-1),\ j = 1, 2, \ldots, M+1.$$

As a result we get a system of $M+1$ nonlinear finite equations with unknown values T_c.

(2) Taking into account the stoichiometric relations between concentrations enables to reduce significantly the dimension of the autonomous system. After that only two concentration equations (for CH_4 and CO_2) were left in the endoblock and one equation (for H_2O)—in the exochannel. Total number of equations in autonomous system (that is combined with nonlinear system of $M+1$ equations) is equal to $3(M+1)+4$, so it is not very large.

(3) If the wall temperature distribution $T_w(\ell)$ is already known, then the numerical problem is reduced to the integration of autonomous discrete system in combination with nonlinear system of equations. Taking into account these considerations, method of "simple iteration" was chosen and it appeared to be very effective. As soon as the integration of autonomous system is completed, then the coefficients $a(l)$ and $b(l)$ for the following linear boundary-value problem (arising from Eq. (3)) are defined more precisely:

$$\frac{d^2 T_w}{dl^2} - a(l) T_w = b(l),$$

$$\frac{dT_w}{dl} = 0 \quad \text{at } \ell = 0 \text{ and } \ell = L. \tag{5}$$

In the following, the autonomous system of equations is again integrated and all iteration cycle is repeated. Important to note that linear boundary-value problem (5) (which is solved during each iteration) is well defined because $a(l) > 0$. This is expressed by the fact of diagonal prevailing in the three-diagonal matrix of coefficients that arises from discrete analog of (5).

(4) Numerical integration of the autonomous system is made with the help of semi-implicit method (second order of accuracy) that is intended for solving "hard" systems of differential equations.

5. Results

Figs. 2–5 demonstrate steady-state numerical solution of the model (continuous curves) that corresponds to the value $k_{ox}^0 = 7$ m/s. The available experimental data is shown in these figures by symbols. Fig. 2 shows temperature profiles along the reactor length. Note that at the reactor inlet, one can observe rather high-temperature differences between the gas and the catalyst and also through the endoblock thickness between the wall ($z = H$) and center ($z = 0$). Taking into account that the thermo-

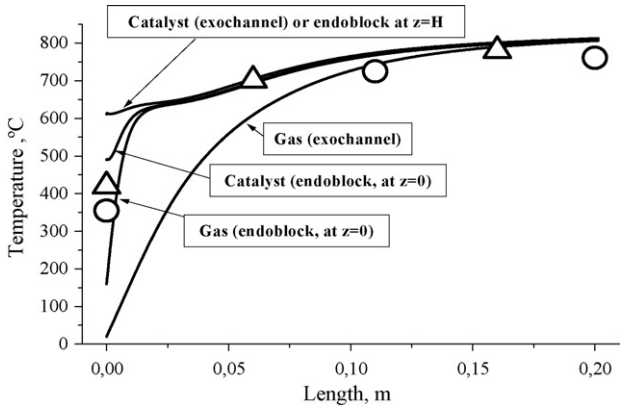

Fig. 2. Temperature profiles along the reactor length. Experimental data are denoted by the following symbols: (△) exothermic channels, (◯) endothermic channels, solid lines denote calculations made at $k_{ox}^0 = 7$ m/s.

couples which were placed inside the exochannel and endoblock contacted both with relatively cold gas flow and relatively hot catalyst, the measured temperatures should be considered as averaged values. So, the agreement between the calculated and the experimental temperatures is good. Towards the reactor outlet all temperatures tend to reach a unique limiting value that

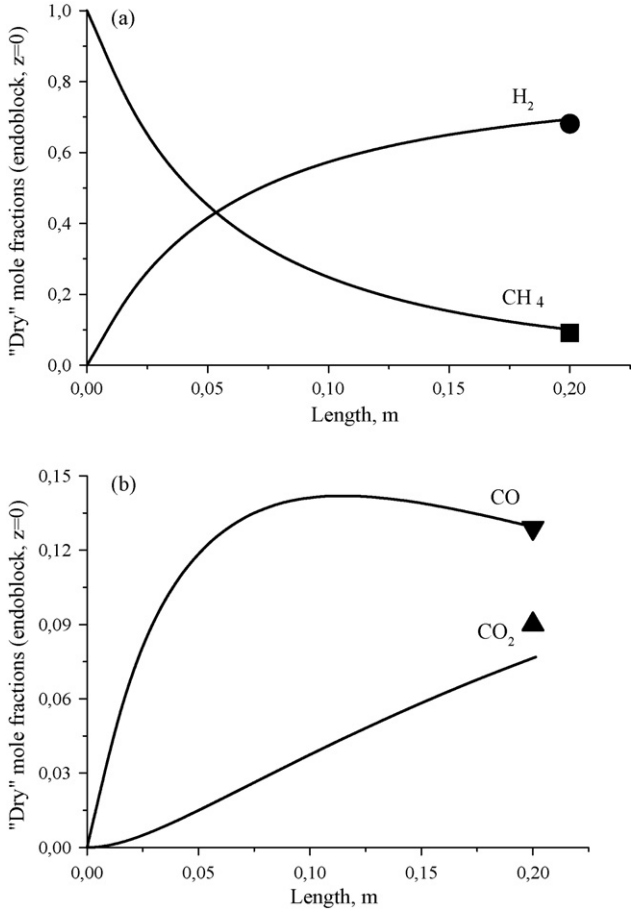

Fig. 3. Profiles of dry gas (mol.) concentrations of H_2, CH_4 (a) and CO, CO_2 (b) calculated in the endoblock (at its plane of symmetry $z = 0$) and the experimental data at the outlet ($k_{ox}^0 = 7$ m/s).

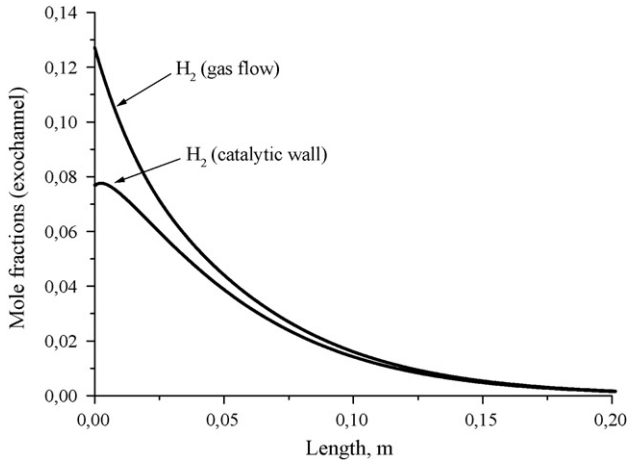

Fig. 4. Calculated profiles along the exochannel for mole fraction of H_2 in the gas flow and at the catalytic wall ($k_{ox}^0 = 7$ m/s).

corresponds to thermodynamic equilibrium and depends only on the inlet temperature (in our case it is approximately 800 °C) and composition.

Fig. 3 shows calculated mole fractions (dry base) for CH_4, H_2, CO, and CO_2 in the reforming channel and the experimental values at the outlet. Methane conversion is rather high but not complete (about 90%). In order to reach higher values of methane conversion at the chosen contact time, more active catalyst is required and/or higher catalyst temperature. The latter can be easily provided by combustion of additional hydrogen in exochannels. But in this case, very high methane conversion may appear ineffective in the sense of optimization of H_2 yield. Fig. 4 compares calculated H_2 mole fractions in the gas flow and at the catalytic wall of exochannel. Significant concentration difference between flow and catalyst surface points out more than 50% control of oxidation reaction rate by external mass transfer. It also explains the large difference between gas and wall temperature in Fig. 2.

Fig. 5 shows calculated transverse profile (across the endoblock $0 < z < H$) of the catalyst temperature at the inlet of reactor. The maximal temperature ~600 °C occurs at the wall ($z = 0.005$ m) at the opposite side of which catalytic combustion

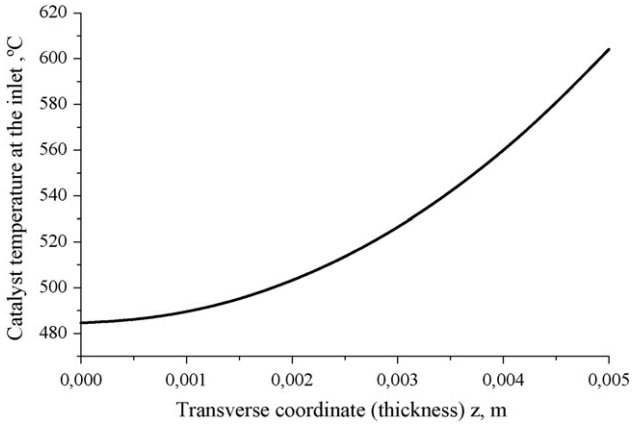

Fig. 5. Calculated transverse catalyst temperature profile (across the endoblock) at the reactor inlet ($k_{ox}^0 = 7$ m/s).

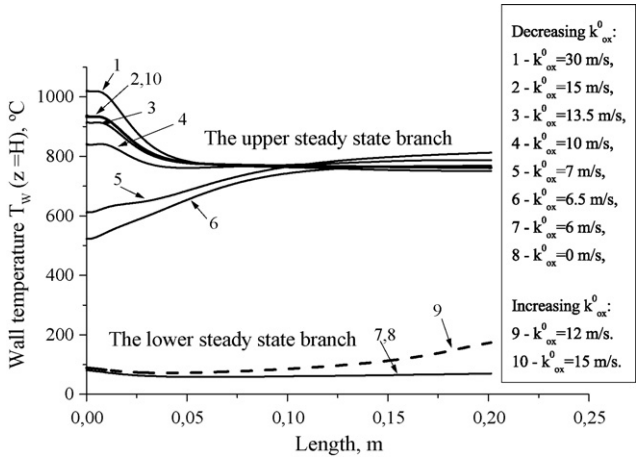

Fig. 6. Calculated profiles of wall temperature T_W under variation of preexponential factor k^0_{ox} for H_2 oxidation rate.

of H_2 takes place. Generated heat is transported by transverse conductivity to the central part of endoblock (more exactly, towards its plane of symmetry $z = 0$). There this heat is partly consumed by endothermic reaction, and partly is spent on the heating of the inlet steam–methane mixture.

It is important to note that the considered reactor regime (for $k^0_{ox} = 7$ m/s) in Figs. 2–5 is not a unique steady state. To say more exactly, there exists hysteresis dependence of the numerical solution on some model parameters. To elucidate this finding, the parameter k^0_{ox} was chosen.

Figs. 6 and 7 show a hysteresis of the exochannel wall temperature regime versus preexponential factor k^0_{ox} for H_2 oxidation rate. The wall temperature profiles (Fig. 6) were obtained for 10 solutions in the range $6 < k^0_{ox} < 30$ m/s. It may be seen that sharply different profiles may correspond to close values of parameter k^0_{ox}, for example, pairs of curves (3, 9) or (6, 7) in Fig. 6. Two steady-state solution branches are distinguished: the lower branch ("cold" regimes) and the upper branch ("hot" regimes). Calculations were made as parameter k^0_{ox} decreased from its maximal value of 30–0 m/s, and then increased back up to 15 m/s. The solution that was found for the previous value of k^0_{ox} was used as the initial approximation for iteration procedure of finding solution for the next value of k^0_{ox}.

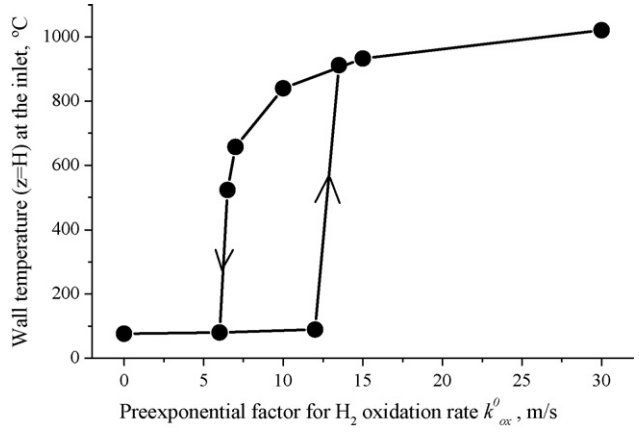

Fig. 7. The hysteresis behavior of the temperature of the wall (at $z = 1$) at the reactor inlet. Hysteresis cycle is constructed by linear interpolation of calculated data in Fig. 6.

In order to demonstrate the hysteresis cycle more clearly, the same calculated results from Fig. 6 were re-plotted in Fig. 7 (the wall temperature at the reactor entrance was chosen as dependent variable and parameter k^0_{ox} as independent variable). The steady-state multiplicity becomes evident. The upper solution branch (normal operation mode of reactor) exists if activity of the oxidation catalyst is rather high ($k^0_{ox} > 6$ m/s). However, if activity is very high ($k^0_{ox} > 15$ m/s), the catalyst undergoes dangerous overheating (hot spot formation) >1000 °C. If the catalyst activity decays to a critical value ($k^0_{ox} \sim 6$ m/s), the reactor operation abruptly changes from the high-temperature mode to the low-temperature one (the reactor extinction occurs). After that the opposite process of ignition is possible only if $k^0_{ox} \sim 13$ m/s. It becomes especially important if we take into account that the estimated real values of parameter k^0_{ox} are just in the range between the points of ignition ($k^0_{ox} \sim 13$ m/s) and extinction ($k^0_{ox} \sim 6$ m/s), i.e. in the domain of steady-state multiplicity. It means that to start up such a reactor an initial heating is required (in order to run up the upper branch of hysteresis cycle in Fig. 7). The start-up of the experimental reactor in practice was done via feeding the exochannels with hydrogen–air mixture (just as methane–steam feed in endoblock was stopped) unless the temperature level 500–600 °C was reached. After that the usual way of feeding may be switched on. Hydrogen oxidation on Pt is sufficiently fast catalytic reaction to start up our reactor in such a manner from room temperatures. Besides the start-up problem, another one exists—high parametric sensitivity and critical phenomena. For example, the considered solution ($k^0_{ox} = 7$ m/s, Figs. 2–5), which is confirmed by experimental data, is placed on the upper branch (Fig. 7) in the dangerous neighborhood with the extinction boundary $k^0_{ox} \sim 6$ m/s. In practice this means that slight variations of activity of oxidation catalyst in the course of a reactor operation may lead to significant changes in temperature regime or even sudden extinction of reactor.

6. Conclusion

There was already known that the models of heat-coupled reactors with *counter-current* oxidation and reforming flows may display extremely complex behavior [1]. The results of this investigation show that the heat-coupled reactor with *co-current* flows also exhibits high parametric sensitivity, hysteresis and points of ignition and extinction. All these features strongly complicate the reactor control and emphasize the role of mathematical modeling. But it should be note that the considered experimental setup does not include a heat recuperation loop and cold gas flow (air + hydrogen) enters into the exochannel. This circumstance may be one of the main reasons leading to the high parametric sensitivity and hysteresis. The authors believe that installation of a recuperative heat exchanger into the pilot setup should increase the flow temperature at the reactor inlet, decrease amount of combusted hydrogen and reduce the reactor parametric sensitivity.

Acknowledgement

Financial support by ISTC Project no. 2291 is gratefully acknowledged.

References

[1] J. Frauhammer, G. Eigenberger, L. Van Hippel, D. Arntz, A new reactor concept for endothermic high-temperature reactions, Chem. Eng. Sci. 54 (1999) 3661–3670.

[2] M. Zanfir, A. Gavriilidis, Catalytic combustion assisted methane steam reforming in a catalytic plate reactor, Chem. Eng. Sci. 58 (2003) 3947–3960.

[3] K. Venkataraman, E.C. Wanat, L.D. Schmidt, Steam reforming of methane and water-gas shift in catalytic wall reactors, AIChE J. 49 (2003) 1277–1284.

[4] G.A. Petrachi, G. Negro, S. Specchia, G. Saracco, P.L. Maffettone, V. Specchia, Combining catalytic combustion and steam reforming in a novel multifunctional reactor for on-board hydrogen production from middle distillates, Ind. Eng. Chem. Res. 44 (2005) 9422.

[5] V.A. Kirillov, N.A. Kuzin, A.B. Shigarov, S.I. Fadeev, O.F. Brizitski, L.N. Khrobostov, A compact hydrocarbon steam reformer with coupling exothermic and endothermic reaction for a fuel processor, Chem. Eng. Trans. 3 (2003) 207–212.

[6] V.A. Kirillov, N.A. Kuzin, A.V. Kulikov, S.I. Fadeev, A.B. Shigarov, V.A. Sobyanin, Thermally coupled catalytic reactor for steam reforming of methane and liquid hydrocarbons: experiment and mathematical modeling, Theor. Found. Chem. Eng. 37 (2003) 276–284.

[7] A.A. Khomenko, L.O. Apelbaum, F.S. Shub, S. Snagovskii, M.I. Temkin, Kinetics of methane reaction with water vapor and the reverse reaction of CO_2 hydrogenation on Ni surface, Kinet. Catal. 12 (1971) 423–429.

[8] S.A.S. Reihani, G.S. Jackson, Effectiveness in catalytic washcoats with multi-step mechanisms for catalytic combustion of hydrogen, Chem. Eng. Sci. 59 (2004) 5937–5948.

[9] V.V. Popovskiy, V.A. Sazonov, G.K. Chermoshentseva, T.L. Panarina, L.F. Eliseeva, Comparative testing of catalysts for deep oxidation, in: Proceedings of 3rd USSR Conference on Catalytic Cleaning of Gases. Part 1, Institute of Catalysis, Novosibirsk, 1981, pp. 80–92 (in Russian).